Failure of the Ingard–Myers boundary condition for a lined duct: An experimental investigation

Ygaël Renou and Yves Aurégan[a)]
Laboratoire d'Acoustique de l'Université du Maine, Unité Mixte de Recherche 6613 Centre National de la Recherche Scientifique, Av. O. Messiaen, 72085 Le Mans Cedex 9, France

(Received 17 October 2010; revised 13 April 2011; accepted 13 April 2011)

This paper deals with experimental investigation of the lined wall boundary condition in flow duct applications such as aircraft engine systems or automobile mufflers. A first experiment, based on a microphone array located in the liner test section, is carried out in order to extract the axial wavenumbers with the help of an "high-accurate" singular value decomposition Prony-like algorithm. The experimental axial wavenumbers are then used to provide the lined wall impedance for both downstream and upstream acoustic propagation by means of a straightforward impedance education method involving the classical Ingard–Myers boundary condition. The results show that the Ingard–Myers boundary condition fails to predict with accuracy the acoustic behavior in a lined duct with flow. An effective lined wall impedance, valid whatever the direction of acoustic propagation, can be suitably found from experimental axial wavenumbers and a modified version of the Ingard–Myers condition with the form inspired from a previous theoretical study [Aurégan *et al.*, J. Acoust. Soc. Am. **109**, 59–64 (2001)]. In a second experiment, the scattering matrix of the liner test section is measured and is then compared to the predicted scattering matrix using the multimodal approach and the lined wall impedances previously deduced. A large discrepancy is observed between the measured and the predicted scattering coefficients that confirms the poor accuracy provided from the Ingard–Myers boundary condition widely used in lined duct applications.
 [DOI: 10.1121/1.3586789]

PACS number(s): 43.28.Py, 43.58.Bh [AH] Pages: 52–60

I. INTRODUCTION

While acoustic liners are extensively used in engineering applications such as aircraft engine systems or automobile mufflers, the acoustical behavior of such systems in the presence of a grazing flow is still a challenging subject due to the complexity of the interaction between sound and flow in the boundary layer over the lined wall. It is often suitable to compute the acoustical propagation by assuming that the flow is potential and to take into account both the effect of the boundary layer (in which large flow velocity gradients and viscothermal and turbulent effects occur) and the effect of the lined wall in the boundary condition of the computation.[1] In this case, it is classically admitted that the acoustic normal displacement and acoustic pressure are continuous across the boundary layer leading to the Ingard[2]–Myers[3] boundary condition. This condition has been widely used in the literature over the past decades.[4–7] Specifically, this condition was used in the computations to deduce the impedance from acoustical measurements.[8–12]

Nevertheless, Aurégan *et al.*[13] and more recently Brambley[14] pointed out that the viscous and turbulent effects near the wall can alter this boundary condition. They demonstrate that the continuity of normal displacement holds only when the acoustic boundary layer thickness is much smaller than the stationary layer thickness, i.e., typically in the high frequency range. At very low frequencies, continuity of mass velocity normal to the lined wall must be applied instead.

Inspired by these theoretical works, this paper mainly aims to provide experimental evidence of the inaccuracy of the results issued from the use of the Ingard–Myers condition in lined duct with uniform flow. The failure of Ingard–Myers condition is observed both from the measurement of axial wavenumbers in the lined duct section and from the scattering matrix.

To this end, experiments were carried out in a duct partly lined with a standard locally reacting liner submitted to a grazing flow. The experimental apparatus is outlined in Sec. II where the measured flow profile is presented. This experimental setup allows the extraction of the experimental axial wavenumbers in the liner test section by means of a linear microphone array located at the upper wall opposite the liner. This setup also allows the measurement of the scattering matrix.

The identified axial wavenumbers related to the least attenuated modes are used in Sec. III to derive the liner impedances in both downstream and reverse flow configurations. To this aim, the mean flow is supposed to be uniform and the Ingard–Myers boundary condition is applied. Significant discrepancies are observed between results in the flow direction and in the reverse flow direction. This invalidates the use of the Ingard–Myers condition associated with uniform flow in our case. Afterward, a modified Ingard–Myers condition (MIMC) is proposed that leads to define an effective lined wall impedance valid for both propagation directions. Section IV describes a multimodal method[9] used to

[a)]Author to whom correspondence should be addressed. Electronic mail: yves.auregan@univ-lemans.fr

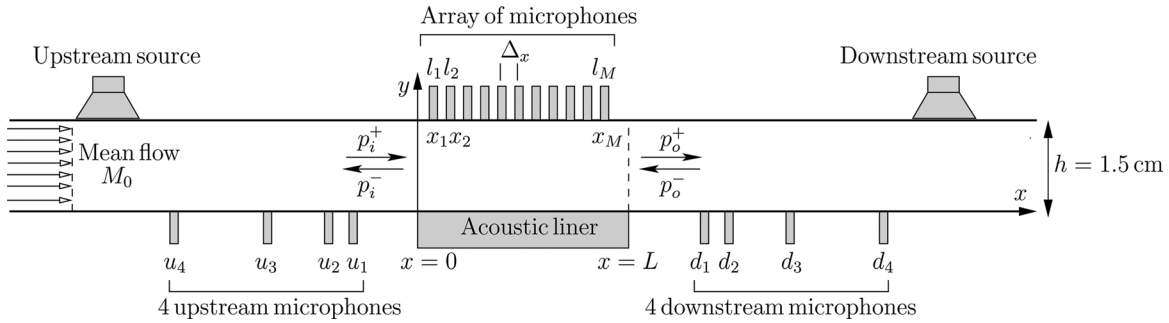

FIG. 1. Schematic view of the experimental setup.

predict the scattering matrix of the liner test section. Finally, a comparison is made between the measured scattering matrix and the predicted multimodal scattering matrix using the Ingard–Myers condition associated with uniform flow. Again significant differences are observed.

II. EXPERIMENTS

A. Experimental apparatus

The test facility (see Fig. 1) used for experiments is described in this section.

The apparatus allows acoustic propagation in a rectangular duct superimposed to a grazing flow over an acoustic liner. At each end of the duct, acoustic sources and anechoic terminations are found. According to the duct dimensions, only two acoustic modes are propagating through the duct: the plane wave and the first order mode along the width of the duct. Due to the centered positioning of the microphones (in the width of the duct), only the plane waves are measured.

Two configurations of microphones are settled in the duct for the following purposes. The scattering matrix is measured by means of 2×4 flush mounted microphones in the lower hard wall downstream and upstream of the liner test section, respectively. It follows that the transmitted and reflected waves can be determined with over-determination to avoid inaccurate measurement when the acoustic wavelength is close to half the distance between two microphones. On the other hand, the axial wavenumbers are measured in the liner test section thanks to an array of 11 flush mounted microphones (denoted l_m with $m = 1,\ldots, M$ in Fig. 1). These microphones are evenly distributed along the x axis spaced out by 2 cm on the hard wall opposite to the acoustic liner.

The acquisition of signals is performed by an Agilent VXI 1432 hardware platform that drives the source excitation synchronously with the acoustic pressure signals recording. A stepped-sine over the frequency range [500–3000] Hz is used with a frequency increment of 10 Hz and a sampling rate of 8192 Hz. A least mean square amplitude and phase estimator is implemented under MATLAB for the post-processing of data.

Experiments were carried out on a conventional acoustic liner widely used in aircraft engine-duct systems (a so-called single degree of freedom liner). This acoustic device is composed of a resistive layer performed by a perforated plate of thickness 1.2 mm with orifices of diameter 1.3 mm and a percent open area of 10.5%. The plate is glued to partitioned air cavities (honeycomb structure) with a depth of 37.5 mm (the cell size is 10 mm). This compound is terminated by a rigid backplate. The dimensions of the sample are 200 mm along the x axis and 100 mm along the z axis.

B. Flow profile in the test duct

The mean flow profile is measured in the test duct by means of a 1 mm diameter pitot tube with EFFA GA064A5-20 static pressure transducer (range 0–20 mbar). The experimental flow velocity is depicted in Fig. 2 for an average Mach number of $M_0 = 0.2$. This profile is compared to the theory for a fully developed turbulent flow in a two-dimensional channel[15]

$$\frac{U}{U_*} = \delta^+, \quad \text{in the laminar sublayer } \delta^+ \leq 11, \tag{1a}$$

$$\frac{U}{U_*} = 2.5 \ln \delta^+ + 5.5, \quad \text{in the logarithmic zone } \frac{2y}{h} \leq 0.2, \tag{1b}$$

$$\frac{U_m - U}{U_*} = 6.3\left(1 - \frac{2y}{h}\right)^2, \quad \text{near the center line } 0.2 \leq \frac{2y}{h} \leq 1, \tag{1c}$$

where U_* is the friction velocity and U_m is the maximum velocity (at the center line of the duct). The values used to fit experimental result are $U_* = 3.14$ m s^{-1} and $U_m = 75.30$

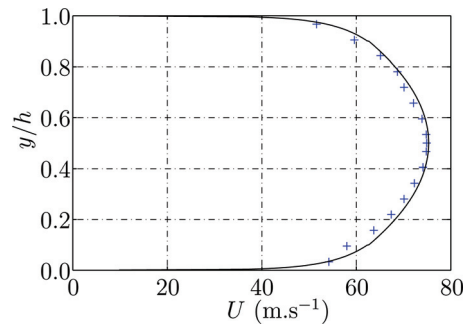

FIG. 2. (Color online) Experimental mean flow profile (plus markers) and theoretical fully developed turbulent flow profile (solid line) with average Mach number of $M_0 = 0.2$.

$\mathrm{m\,s^{-1}}$. The reduced coordinate δ^+ is given by $\delta^+ = yU_*/v$ with $v = 1.51\times10^{-5}\ \mathrm{m^2\,s^{-1}}$ the kinematic viscosity of air at 20 °C. The limit between the laminar sublayer and the logarithmic zone is found to be $\delta^+ = 11$, i.e., $y \approx 0.052$ mm. For $M_0 = 0.2$, the mean Reynolds number is given by $R_e = U_0 h/v = 6.74\times10^4$. The y-average mean flow velocity $U_0 = 67.8\ \mathrm{m\,s^{-1}}$ is related to the mean Mach number by $M_0 = U_0/c_0$. For the frequency range of interest in this paper, it can be noted the following values for the acoustic boundary layer

$$\delta_a \approx 0.10\ \text{mm} \quad \text{at} \quad f = 500\ \text{Hz}, \tag{2a}$$

$$\delta_a \approx 0.06\ \text{mm} \quad \text{at} \quad f = 1500\ \text{Hz}, \tag{2b}$$

$$\delta_a \approx 0.04\ \text{mm} \quad \text{at} \quad f = 3000\ \text{Hz}, \tag{2c}$$

wherein f denotes the frequency of sound.

The good agreement between the experimental and theoretical flow profiles shows that the flow in the duct can be considered as a fully developed turbulent flow.

C. Method for the measurement of the axial wavenumbers in the liner test section

The method outlined in the following text refers to the well-known Kumaresan and Tufts[16] (KT) approach, which is slightly modified for our application. Here the aim is to estimate the axial wavenumbers k_0^+ (respectively, k_0^-) corresponding to the least attenuated waves propagating through the liner test section in the downstream (respectively, upstream) direction with the presence of a grazing flow by the use of microphone array.[17] k_0^+ is extracted from the measurement with an active upstream source (the downstream source is turned off) and k_0^- from the measurement with an active downstream source (the upstream source is turned off).

According to the modal decomposition in a 2D duct, the pressure field at the hard upper wall opposite to the lined wall reduces to

$$p_m = \sum_{n=0}^{\infty} b_n^+ e^{-\mathrm{i}k_n^+(x_m - x_1)} + \sum_{n=0}^{\infty} b_n^- e^{-\mathrm{i}k_n^-(x_m - x_1)}, \quad m = 1, \ldots\ldots, M, \tag{3}$$

where $k_n^\pm$ are the axial wavenumbers in the liner test section, $b_n^\pm$ are the complex waves amplitudes, $x_m - x_1 = (m-1)\Delta_x$ is the location along the upper wall where the pressure $p_m = p(x_m, y = 1)$ is measured, and M is the number of microphones mounted flush at the inner surface of the upper wall in the liner test section.

From now on, the dimensionless form of the quantities of interest are introduced according to

$$\begin{array}{lll} p' = p/\left(\rho_0 c_0^2\right), & k_n'^{\pm} = k_n^\pm h, & x' = x/h, \\ y' = y/h, & \Delta_x' = \Delta_x/h, & \omega' = \frac{\omega h}{c_0}, \end{array} \tag{4}$$

wherein the superscript $'$ symbol denotes the quantities without dimension, h is the transverse size of the duct, ρ_0 and c_0 are the density of fluid and the velocity of sound, respectively, and ω is the angular frequency of sound. In the following, $'$ is dropped for convenience.

Equation (3) can be put in a compact parametric model form

$$p_m = \sum_{n=1}^{N} a_n s_n^{m-1}, \quad m = 1, \ldots\ldots, M. \tag{5}$$

The method outlined below consists in identifying the axial wavenumbers $k^\pm$ from the poles $s_n = e^{-\mathrm{i}k_{n-1}^\pm \Delta x}$ via the KT algorithm.

Choosing a parameter K (it can be found in the literature[18] that choosing $K = 3M/4$ provides the more optimized results, which is assumed to be also the case in our application) such that $\min(M - K, K) \geq N$, the recursive relations between the transfer functions $H_{l_m l_{ref}} = p_m/p_{ref}$ ($l_{ref} = l_1$ for instance) at successive locations along the upper wall are obtained by (see the Appendix)

$$H_{l_m l_{ref}} = -\sum_{n=1}^{K} c_n H_{l_{m+n} l_{ref}} \tag{6}$$

and are reduced to a matrix form equation

$$\mathbf{Ac} = -\mathbf{b}, \tag{7}$$

where $\mathbf{A}$ is a $(M - K) \times K$ Hankel data matrix. $\mathbf{b}$ is a $(M - K) \times 1$ column vector.

The vector of the prediction coefficients $\mathbf{c}$ is determined such as

$$\mathbf{c} = -\mathbf{A}^\dagger \mathbf{b} \tag{8}$$

$$= -\left(\mathbf{A}^H \mathbf{A}\right)^{-1} \mathbf{A}^H \mathbf{b} \tag{9}$$

where $\mathbf{A}^\dagger$ is the pseudo-inverse of $\mathbf{A}$ and $\mathbf{A}^H$ denotes the conjugate transpose of $\mathbf{A}$.

The singular value decomposition of $\mathbf{A}$ leads to

$$\mathbf{A} = \mathbf{U\Sigma V}^H, \tag{10}$$

$$\mathbf{A}^\dagger = \mathbf{V}\ \Sigma^{-1}\mathbf{U}^H, \tag{11}$$

where $\mathrm{diag}[\mathbf{\Sigma}] = \{\Sigma_1, \ldots, \Sigma_Q, \Sigma_{Q+1}, \ldots, \Sigma_K\}^T$ is the vector of the singular values arranged in the decreasing order. $\mathbf{U}$ and $\mathbf{V}$ are the left and right singular vectors, respectively.

The basic idea underlying the KT method is to reduce the measurement noise by considering the reduced rank approximation of $\mathbf{A}$ such that

$$\mathbf{A}_Q = \mathbf{U\Sigma}_Q \mathbf{V}^H \tag{12}$$

with $\mathrm{diag}[\Sigma_Q] = \{\Sigma_1, \ldots, \Sigma_Q, 0, \ldots, 0\}^T$, $Q \leq M - K$. Then an estimate of the prediction coefficients is given by

$$\mathbf{c}_Q = -\mathbf{A}_Q^\dagger \mathbf{b}. \tag{13}$$

The resolution of the characteristic equation (see the Appendix)

$$C(z) = 1 + \sum_{n=1}^{K} c_n z^n \tag{14}$$

provides the roots $z_n = 1/s_n$ with s_n the poles of Eq. (5). The roots that lie outside the unit circle in the complex z-plane correspond to physical modes, whereas the roots that lie inside the unit circle are due to extraneous noise or spurious modes.

D. Method for the measurement of the acoustic scattering matrix

The scattering matrix $\mathbf{S}$ relates the scattered pressure amplitudes p_i^- and p_o^+ to the incident pressure amplitudes p_i^+ and p_o^- of the plane waves in the rigid duct as follows

$$\begin{pmatrix} p_o^+ \\ p_i^- \end{pmatrix} = \mathbf{S} \begin{pmatrix} p_i^+ \\ p_o^- \end{pmatrix} = \begin{bmatrix} T^+ & R^- \\ R^+ & T^- \end{bmatrix} \begin{pmatrix} p_i^+ \\ p_o^- \end{pmatrix}, \tag{15}$$

where T^+ and T^- are the anechoic transmission coefficients, R^+ and R^- are the anechoic reflection coefficients, and the subscripts i and o indicate the inlet and the outlet of the liner test section, respectively (see Fig. 1). The scattering matrix is measured in a similar manner as described by Aurégan *et al.*[9] and is referred to as the two-source method.

III. ANALYSIS OF RESULTS OBTAINED FROM THE AXIAL WAVENUMBERS IN THE LINED DUCT TEST SECTION

A. Analysis of results with the Ingard–Myers boundary condition

Assuming a locally reacting liner, its impedance Z_w is expressed as

$$Z_w = \frac{p}{\mathbf{v}_w \cdot \mathbf{n}}, \qquad y = 0, 0 < x < L/h, \tag{16}$$

wherein $\mathbf{n}$ is the outward normal vector pointing into the wall and $\mathbf{v}_w$ is the acoustic velocity at the lined wall. As there is no mean flow at the wall, $\mathbf{v}_w$ is linked to the acoustic displacement $\boldsymbol{\xi}_w$ at the wall by

$$\mathbf{v}_w \cdot \mathbf{n} = \frac{\partial \boldsymbol{\xi} w}{\partial t} \cdot \mathbf{n}, \quad \text{at} \quad y = 0. \tag{17}$$

Assuming a thin shear layer close to the lined wall, the acoustic normal displacement as well as the acoustic pressure can be considered constant across the boundary layer. Then, the transverse kinematic condition is written as

$$\begin{aligned} \mathbf{v}_\varepsilon \cdot \mathbf{n} &= \left(\frac{\partial}{\partial t} + M_0 \frac{\partial}{\partial x}\right) \boldsymbol{\xi}_\varepsilon \cdot \mathbf{n} \\ &= \left(\frac{\partial}{\partial t} + M_0 \frac{\partial}{\partial x}\right) \boldsymbol{\xi}_w \cdot \mathbf{n}, \end{aligned} \tag{18}$$

where $\mathbf{v}_\varepsilon$ and $\boldsymbol{\xi}_\varepsilon$ denote the velocity and the displacement just above the thin boundary layer. When $\varepsilon \to 0$, then $\mathbf{v}(x, y = 0) \cdot \mathbf{n} \to \mathbf{v}_\varepsilon \cdot \mathbf{n}$ and $p(0) \to p_\varepsilon = p_w$ leading to the lined wall boundary condition

$$\mathrm{i}\omega(\mathbf{v}(x,0) \cdot \mathbf{n}) = \left(\mathrm{i}\omega + M_0 \frac{\partial}{\partial x}\right)\left(\frac{p(x,0)}{Z_w}\right), \quad 0 < x < L/h, \tag{19}$$

where $\mathrm{i}\omega$ stands for the time derivative for an harmonic time dependence $e^{\mathrm{i}\omega t}$.

Using the Euler equation in the y-direction, Eq. (19) is transformed into a relation between the acoustic pressure, its first transverse derivative, and the lined wall impedance

$$\frac{\partial p}{\partial y} = \left(\frac{1}{\mathrm{i}\omega Z_w}\right)\left(\mathrm{i}\omega + M_0 \frac{\partial}{\partial x}\right)^2 p, \quad y = 0, \ 0 < x < L/h. \tag{20}$$

The relation (19) is called the Ingard–Myers boundary condition[2,3] for a plane boundary. For convenience, the Ingard–Myers boundary condition is used under the form (20) instead of (19) in the following.

The pressure is written as $p(x,y) = P(y)\mathrm{e}^{\mathrm{i}(\omega t - kx)}$. For a uniform mean flow, substituting the pressure in the convected wave equation leads to

$$\frac{\mathrm{d}^2 P(y)}{\mathrm{d}y^2} + k_y^2 P(y) = 0,$$

where

$$k_y^2 = (\omega - M_0 k)^2 - k^2. \tag{21}$$

The transverse pressure can be written in the case of a rigid upper wall as $P(y) = b \cos(k_y(y-1))$. Applying the Ingard–Myers condition [Eq. (20)] leads to

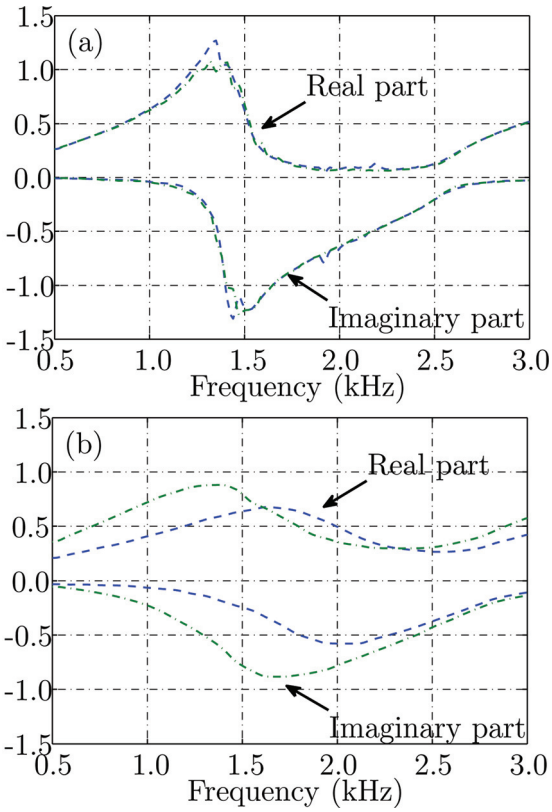

FIG. 3. (Color online) Experimental axial wavenumbers k_0^+ (dashed line) and $-k_0^-$ (dashed-dotted line). (a) $M_0 = 0$, (b) $M_0 = 0.2$. The parameters used in Sec. II C for experimental extraction of $k_0^\pm$ are $K = 8$, $M = 11$, and $Q = 2$.

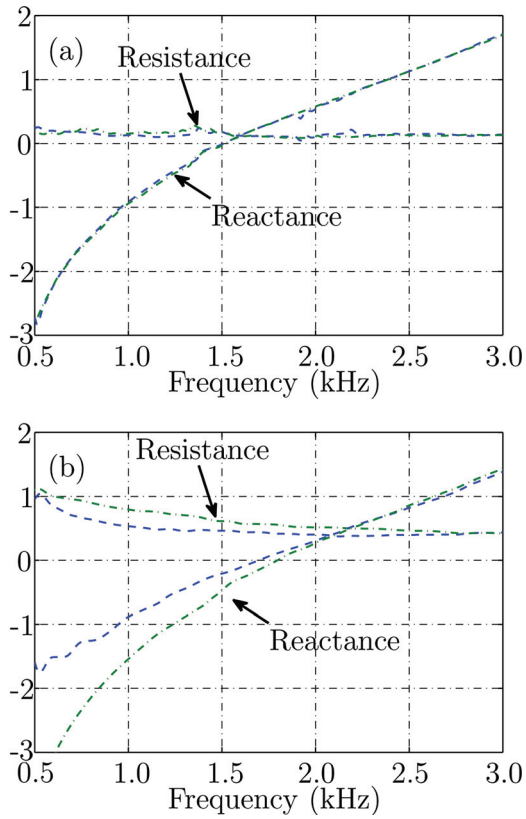

FIG. 4. (Color online) Specific acoustic impedance of the lined wall $Z_w = Z^{\mathrm{I}}$ (dashed line) and $Z_w = Z^{\mathrm{I}}$ (dashed-dotted line) calculated with Eqs. (22) and (21). (a) $M_0 = 0$, (b) $M_0 = 0.2$.

$$k_y \tan(k_y) = \frac{(\mathrm{i}\omega - \mathrm{i}M_0 k)^2}{\mathrm{i}\omega Z_w}. \tag{22}$$

These equations give an explicit relation between the unknown impedance Z_w of the lined wall and the measured axial wavenumbers k in the lined duct test section.

For the sake of accuracy, the lined wall impedance is calculated only with the axial wavenumbers of the least attenuated waves, namely, k_0^+ and k_0^-. The latter are shown in Fig. 3(a) for $M_0 = 0$ and in Fig. 3(b) for $M_0 = 0.2$ (for clarity, k_0^+ is compared to $-k_0^-$). They correspond to the predominant modes in the duct, traveling in downstream and upstream directions (in the flow direction and in the reverse direction of the flow, respectively).

Hence the measurement with active upstream source (while the downstream source is switched off) provides the lined wall impedance denoted Z^{I} derived from k_0^+, and the measurement with active downstream source (while the upstream source is switched off) provides Z^{II} derived from k_0^-.

The real and imaginary parts of the lined wall impedances Z^{I} and Z^{II} are depicted in Fig. 4(a) for $M_0 = 0$ and in Fig. 4(b) for $M_0 = 0.2$.

Without flow, the two impedance curves are close as one can expect. At $M_0 = 0.2$, a large discrepancy occurs between the two curves.

Clearly the fact that two different values of the impedance are obtained for two different directions of the propagation is incompatible with the model used. Thus the use of the Ingard–Myers boundary condition associated with uniform flow is not satisfactory with our measurements. Accordingly, these assumptions cannot be applied to deduce accurately the impedance. It may be noted that this phenomenon could not be observed by other experimentalists because they only use one upstream source.[8,12]

B. Analysis of results with the modified version of Ingard–Myers boundary condition

In Ref. 13, Aurégan *et al.* have theoretically demonstrated at low Mach number and for simple flow profiles with constant molecular viscosity through the shear layer that an extra parameter, say, β_v, can be introduced in the lined wall boundary condition to take into account the transfer of momentum into the lined wall induced by molecular and turbulent viscosities.

From this theoretical analysis, the transverse kinematic condition [Eq. (18)] is modified as

$$\boldsymbol{v}_\varepsilon \cdot \mathbf{n} = \left(\mathrm{i}\omega + (1-\beta_v) M_0 \frac{\partial}{\partial x}\right) \boldsymbol{\xi}_w \cdot \mathbf{n}. \tag{23}$$

When $\beta_v = 0$, Eq. (23) recovers the classical Ingard–Myers boundary condition, i.e., the continuity of normal acoustic displacement, whereas $\beta_v = 1$ yields to the continuity of acoustic mass velocity.

The previous relation leads to a modified Ingard–Myers boundary condition (MIMC) expressed as

$$\frac{\partial p}{\partial y} = \frac{1}{\mathrm{i}\omega Z_w}\left[\mathrm{i}\omega + (1-\beta_v) M_0 \frac{\partial}{\partial x}\right]\left[\mathrm{i}\omega + M_0 \frac{\partial}{\partial x}\right] p, \tag{24}$$

at $y = 0$ and $0 < x < L/h$.

The modified version of Ingard–Myers boundary condition [Eq. (24)] leads to also modify Eq. (22) as

$$k_y \tan(k_y) = \frac{(\mathrm{i}\omega - \mathrm{i}(1-\beta_v) M_0 k)(\mathrm{i}\omega - \mathrm{i}M_0 k)}{\mathrm{i}\omega Z_w}. \tag{25}$$

The parameter β_v is obtained by constraining the modified Ingard–Myers boundary condition to give a unique effective lined wall impedance Z_{eff}, valid whatever the direction of wave propagation.

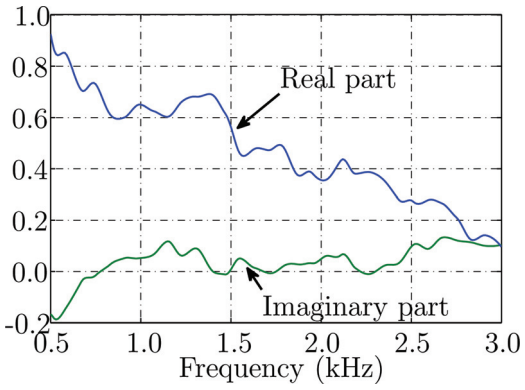

FIG. 5. (Color online) Real and imaginary parts of β_v^{exp} with $M_0 = 0.2$.

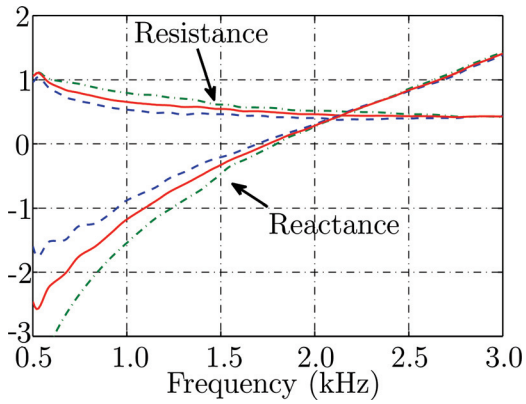

FIG. 6. (Color online) Specific acoustic impedance of the lined wall $Z_w = Z^{\mathrm{I}}$ (dashed line) with $\beta_v = 0$, $Z_w = Z^{\mathrm{I}}$ (dashed-dotted line) with $\beta_v = 0$ and $Z_w = Z_{eff}$ (solid line) calculated with Eqs. (21) and (25) and $\beta_v = \beta_v^{exp}$ (see Fig. 5) with $M_0 = 0.2$.

Thus k_0^+ and k_0^- experimentally determined, are introduced into Eq. (25)

$$X_1 = \frac{\mathrm{i}\omega}{Z_{eff}}\left[1 - (1-\beta_v)M_1\frac{k_0^+}{\omega}\right] Y_1,$$
$$X_2 = \frac{\mathrm{i}\omega}{Z_{eff}}\left[1 - (1-\beta_v)M_2\frac{k_0^-}{\omega}\right] Y_2,$$

where $X_1 = k_{y0}^+ \tan\left(k_{y0}^+\right), X_2 = k_{y0}^- \tan\left(k_{y0}^-\right), Y_1 = 1 - \frac{M_1 k_0^+}{\omega}$, $Y_2 = 1 - \frac{M_2 k_0^-}{\omega}, M_1 = M_0$ and $M_2 = -M_0$. k_{y0}^+ and k_{y0}^- are determined with the help of Eq. (21)

After elimination of the unknown impedance Z_{eff} in the previous equations, one readily finds the factor β_v given by

$$\beta_v = \frac{\alpha_2}{\alpha_1}, \tag{26}$$

with

$$\alpha_1 = \frac{X_1}{X_2}\frac{M_0 k_0^-}{\omega} + \frac{Y_1}{Y_2}\frac{M_0 k_0^+}{\omega},$$

$$\alpha_2 = \frac{X_1}{X_2}\left(1 + \frac{M_0 k_0^-}{\omega}\right) - \frac{Y_1}{Y_2}\left(1 - \frac{M_0 k_0^+}{\omega}\right).$$

The real and imaginary parts of the experimental parameter β_v, derived from Eq. (26) with the use of the experimental wavenumbers in the lined duct test section, is denoted β_v^{exp} from now on. This latter is depicted in Fig. 5 for $M_0 = 0.2$.

It can be observed that the real part of the experimental factor β_v^{exp} is decreasing as the frequency increases. This result fits with the theoretical analysis given by Aurégan *et al.*[13] The modified boundary condition tends to recover the Ingard–Myers boundary condition in the high frequency range.

The value of β_v^{exp} is used in Eqs. (21) and (25) to obtain the effective lined wall impedance denoted Z_{eff} accounting for the modified version of the Ingard–Myers boundary condition. The resulting effective lined wall impedance Z_{eff} is presented in Fig. 6 conjointly with Z^{I} and Z^{II}.

IV. ANALYSIS OF RESULTS OBTAINED FROM SCATTERING MATRICES

A second measurement, independent of the measurement used in previous section, has been made. It consists in the measurement of the scattering matrix.[9–11] This measurement is compared with the scattering matrix computed for a uniform mean flow and Ingard–Myers condition either with Z^{I} or Z^{II}. The multimodal method used to predict the scattering matrix is briefly outlined in the following text. The reader is invited to refer to a previous paper for complete details.[9]

A. The predicted scattering matrix using the multimodal method

The problem of acoustic propagation in a 2D channel with uniform flow is here described in term of displacement potential, denoted ϕ. Without incident vorticity, the displacement potential obeys to the 2D convective wave equation

$$\frac{\mathrm{D}^2\phi}{\mathrm{D}t^2} - \nabla^2\phi = 0 \tag{27}$$

where $\mathrm{D}/\mathrm{D}t = [\mathrm{i}\omega + M_0(\partial/\partial x)]$ is the convective derivative.

At the rigid walls, the normal acoustic velocity vanishes. This could be expressed in term of acoustic displacement potential as

$$\frac{\partial\phi}{\partial y} = 0. \tag{28}$$

At the lined wall of the duct, the Ingard–Myers boundary condition is

$$\frac{\partial\phi}{\partial y} = \frac{1}{\mathrm{i}\omega Z_w}\left[\mathrm{i}\omega + M_0\frac{\partial}{\partial x}\right]^2\phi. \tag{29}$$

Here the acoustic displacement potential is preferred to the acoustic pressure because of the regularity of ϕ near an abrupt change in wall impedance contrary to the pressure $p = -\mathrm{D}^2\phi/\mathrm{D}t^2$, which is then singular in this case.[9] Using the pressure variable, some specific mode-matching method is needed at the rigid-soft wall interfaces.[7] For the sake of simplicity, the scattering matrix denoted $\mathbf{S}_\phi$ is first computed with displacement potential formulation, and then the scattering matrix $\mathbf{S}$ is computed in term of pressure variable afterward.

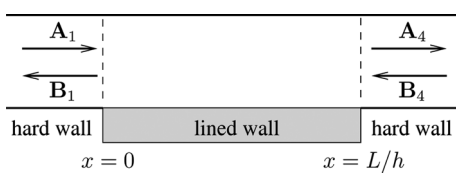

FIG. 7. Notations for amplitudes of the transmitted and reflected waves at each interface between hard and lined walls.

Using the multimodal approach as described in Ref. 9, the scattering matrix relates the vector amplitude of the incoming waves (denoted $\mathbf{A}_1$ and $\mathbf{B}_4$ in Fig. 7) to the vector amplitude of the outcoming waves (denoted $\mathbf{B}_1$ and $\mathbf{A}_4$ in Fig. 7) upstream and downstream of the lined duct test section as

$$\begin{pmatrix} \mathbf{A}_4 \\ \mathbf{B}_1 \end{pmatrix} = \underbrace{\begin{bmatrix} \mathbf{T}_\phi^+ & \mathbf{R}_\phi^- \\ \mathbf{R}_\phi^+ & \mathbf{T}_\phi^- \end{bmatrix}}_{=[\mathbf{S}_\phi]} \begin{pmatrix} \mathbf{A}_1 \\ \mathbf{B}_4 \end{pmatrix}. \tag{30}$$

In this paper, we are interested only by the reflection and transmission coefficients for the plane waves upstream and downstream of the lined duct test section given by

$$T_\phi^+ = \frac{\mathbf{A}_4(1)}{\mathbf{A}_1(1)} = \mathbf{S}_\phi(1,1), \tag{31a}$$

$$R_\phi^- = \frac{\mathbf{A}_4(1)}{\mathbf{B}_4(1)} = \mathbf{S}_\phi(1,\ 2N+1), \tag{31b}$$

$$R_\phi^+ = \frac{\mathbf{B}_1(1)}{\mathbf{A}_1(1)} = \mathbf{S}_\phi(2N+1,1), \tag{31c}$$

$$T_\phi^- = \frac{\mathbf{B}_1(1)}{\mathbf{B}_4(1)} = \mathbf{S}_\phi(2N+1,2N+1), \tag{31d}$$

where $2N$ total modes are considered (N upstream propagating modes and N downstream propagating modes). It should be noted that the separation of the upstream and downstream propagating modes has to be done with care (usually given by the imaginary part of the wavenumbers) because some hydrodynamic (or unstable) modes can exist.

Then the coefficients of the scattering matrix in term of acoustic pressure for the plane waves are easily retrieved from

$$T^\pm = T_\phi^\pm, \tag{32a}$$

$$R^\pm = R_\phi^\pm \left(\frac{1 \pm M_0^2}{1 \mp M_0^2}\right). \tag{32b}$$

B. Comparison between the measured and the predicted scattering matrix computed with the conventional Ingard–Myers boundary condition

The multimodal scattering matrix with a number of 50 modes ($N=25$ downstream modes and $N=25$ upstream modes), which is enough to ensure the convergence of the scattering coefficients (with converged error $<1\%$), is computed according to the method briefly outlined in the previous section with a lined wall impedance value such that $Z_w = Z^{\mathrm{I}}$ and $Z_w = Z^{\mathrm{II}}$, respectively.

As one can expect in the no flow configuration, good agreement is observed between the measured and the predicted scattering matrix [see Figs. 8(a) and 8(b)]. The difference occurring around 1.5 kHz on $|T^+|$ is due to the

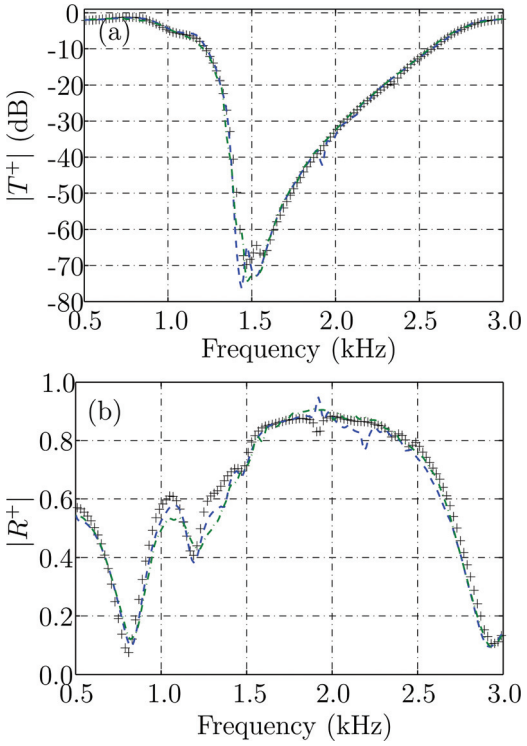

FIG. 8. (Color online) Comparison between the measured (plus markers) and the predicted scattering matrix calculated with the Ingard–Myers boundary condition ($\beta_v = 0$) for $Z_w = Z^{\mathrm{I}}$ (dashed lines) and for $Z_w = Z^{\mathrm{II}}$ (dashed-dotted lines) at $M_0 = 0$. (a) Magnitude of T^+. (b) Magnitude of R^+.

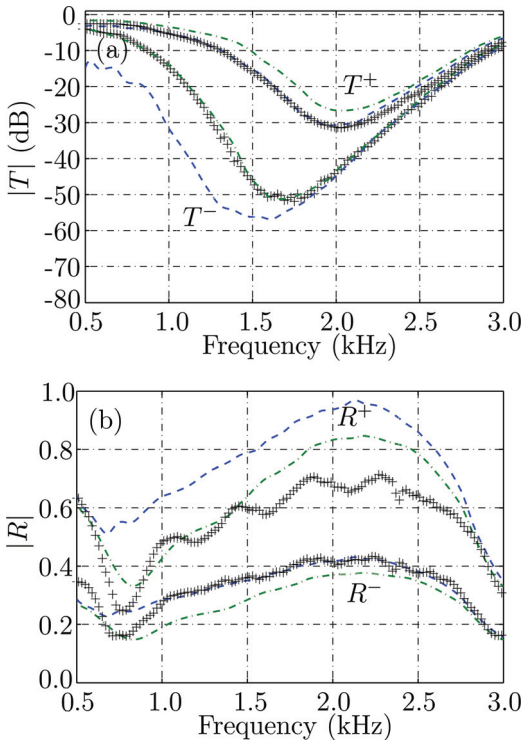

FIG. 9. (Color online) Comparison between the measured (plus markers) and the predicted scattering matrix calculated at $M_0 = 0.2$ with the Ingard–Myers boundary condition ($\beta_v = 0$) for $Z_w = Z^{\mathrm{I}}$ (dashed lines) and for $Z_w = Z^{\mathrm{II}}$ (dashed-dotted lines). (a) Magnitude of T^+ and T^-. (b) Magnitude of R^+ and R^-.

accuracy limit of the acquisition system (which nevertheless permits measurement of an attenuation up to 70 dB).

$|T^-|$ and $|R^-|$ are intentionally not presented in Figs. 8(a) and 8(b) because the scattering matrix is reciprocal and symmetric in the no flow case, i.e., $T^+ \approx T^-$ and $R^+ \approx R^-$.

With flow ($M_0 = 0.2$), Figs. 9(a) and 9(b) show that a large discrepancy occurs, in particular, on the predicted transmission and reflection coefficients when using alternatively Z^{I} or Z^{II}. More precisely, when Z^{I} is used, there is a good fit of the experimental T^+ and R^- with the computed values. On the other hand, using Z^{II} leads to a good agreement with T^-. The reflection coefficient R^+ is accurately predicted neither with Z^{I} nor with Z^{II}.

Thus neither Z^{I} nor Z^{II} can provide a good agreement with both T^+ and T^-. If the value Z_{eff} is used instead (this approach is not in coherence with the assumptions made for the calculation, i.e., the use of Ingard–Myers condition associated with a uniform flow), there is not a good agreement on all the coefficients especially the reflection coefficients.

Again, those results show that the uniform flow assumption associated with the use of Ingard–Myers condition is inadequate to predict measurements for both downstream and upstream results.

V. CONCLUSION

In this paper, two different experiments were performed with a conventional perforated liner widely used in aeronautical applications. Both show the inadequacy of using a uniform mean flow assumption associated with the classical Ingard–Myers boundary condition. From these experimental results, the use of the Ingard–Myers condition in small ducts, like the duct used in this study and more generally in the ducts used in the impedance eduction techniques, seems to be questionable.

The possibilities to this work are numerous. Experiments have been carried out with only one acoustic liner and for a unique flow rate. More experiments on different linings with different flow boundary layer thicknesses are needed to provide benchmark data concerning the β_v factor. Furthermore, a mathematical analysis is also required concerning the behavior of the MIMC in terms of stability, causality, etc. Last, the introduction of the MIMC in the duct acoustic models leads also to a modified mode-matching scheme that has to be developed.

ACKNOWLEDGMENTS

This work was supported in part by a grant from ARCOCE program.

APPENDIX

The parametric model [Eq. (5)] for the pressure field at the upper hard wall in the lined part of the duct can be considered as a space state model defined by

$$\mathbf{X}_{m+1} = \mathbf{F}\mathbf{X}_m, \quad m = 1, \ldots, M \tag{A1a}$$

$$p_m = \mathbf{1}\mathbf{X}_m, \tag{A1b}$$

where $\mathbf{X}_{m+1}$ and $\mathbf{X}_m$ are the vectors of state variables with $\mathbf{X}_1 = \{a_1, \ldots, a_N\}^T$, $\mathbf{F}$ is a $N \times N$ matrix that contains the poles s_n on diagonal

$$\mathbf{F} = \begin{bmatrix} s_1 & & 0 \\ & \ddots & \\ 0 & & s_N \end{bmatrix}, \tag{A2}$$

and $\mathbf{1}$ is the identity row vector.

If the square matrix $\mathbf{F}$ admits as a characteristic equation

$$C(\lambda) = \det|\lambda\mathbf{I} - \mathbf{F}| = c_0 + c_1\lambda^1 + c_2\lambda^2 + \cdots + c_N\lambda^N, \tag{A3}$$

then the Cayley-Hamilton theorem states that $\mathbf{F}$ is itself root of Eq. (A3) such that

$$C(\mathbf{F}) = 0. \tag{A4}$$

It follows that

$$c_0\mathbf{I} + c_1\mathbf{F}^1 + \cdots + c_{N-1}\mathbf{F}^{N-1} + c_N\mathbf{F}^N = \mathbf{0}, \tag{A5}$$

where $c_0 = 1$.

Equation (A1b) provides

$$\begin{cases} \mathbf{X}_m = \mathbf{I}\mathbf{X}_m \\ \mathbf{X}_{m+1} = \mathbf{F}^1\mathbf{X}_m \\ \mathbf{X}_{m+2} = \mathbf{F}^2\mathbf{X}_m \\ \quad\vdots \qquad\quad \vdots \\ \mathbf{X}_{m+N} = \mathbf{F}^N\mathbf{X}_m. \end{cases} \tag{A6}$$

Multiplying the previous equations by $c_0, c_1, \ldots, c_{N-1}, c_N$, respectively, and then summing the resulting relations gives

$$\sum_{n=0}^{N} c_n\mathbf{X}_{m+n} = \left(\sum_{n=0}^{N} c_n\mathbf{F}^n\right)\mathbf{X}_m. \tag{A7}$$

From Eq. (A5) it can be seen that Eq. (A7) reduces to

$$\sum_{n=0}^{N} c_n\mathbf{X}_{m+n} = \mathbf{0}, \tag{A8}$$

which provides

$$\sum_{n=1}^{N} c_n\mathbf{X}_{m+n} = -c_0\mathbf{X}_m. \tag{A9}$$

Using Eq. (A1b) with Eq. (A9) leads to the equations of linear prediction

$$p_m = -\sum_{n=1}^{N} c_n p_{m+n}, \tag{A10}$$

wherein $c_0 = 1$.

Dividing Eq. (A10) by p_{ref}, one finally obtains

$$H_{l_m l_{ref}} = -\sum_{n=1}^{N} c_n H_{l_{m+n} l_{ref}}. \tag{A11}$$

This is the recursive relation equivalent to Eq. (6) by replacing N by K the prediction order chosen such that min $(M-K, K) \geq N$.

The roots of Eq. (A3)

$$C(z) = c_0 + c_1 z^1 + c_2 z^2 + \cdots + c_{N-1} z^{N-1} + c_N z^N = 1 + \sum_{n=1}^{N} c_n z^n, \tag{A12}$$

provide the poles $s_n = 1/z_n$. Equation (A12) is similar to Eq. (14), considering the summation with upper bound K instead of N, without loss of generality.

[1]A. H. Nayfeh, J. E. Kaiser, and D. P. Telionis, "Acoustics of aircraft engine-duct systems," AIAA J. **13**, 130–153 (1975).

[2]U. Ingard, "Influence of fluid motion past a plane boundary on sound reflection, absorption, and transmission," J. Acoust. Soc. Am. **31**, 1035 (1959).

[3]M. Myers, "On the acoustic boundary condition in the presence of flow," J. Sound Vib. **71**, 429–434 (1980).

[4]W. Eversman, "Theoretical models for duct acoustic propagation and radiation," in *Aeroacoustics of Flight Vehicles: Theory and Practice. Noise Control*, edited by H. H. Hubbard, NASA Document No. 199200005564 (1991) Vol. 2, pp. 101–163.

[5]S. W. Rienstra, "Sound propagation in slowly varying lined flow ducts of arbitrary cross- section," J. Fluid Mech. **495**, 157–173 (2003).

[6]W. Bi, V. Pagneux, D. Lafarge, and Y. Aurégan, "Modelling of sound propagation in a non-uniform lined duct using a multi-modal propagation method," J. Sound Vib. **289**, 1091–1111 (2006).

[7]G. Gabard and R. Astley, "A computational mode-matching approach for sound propagation in three-dimensional ducts with flow," J. Sound Vib. **315**, 1103–1124 (2008).

[8]W. Watson, M. Jones, and T. Parrott, "Validation of an impedance education method in flow," AIAA J. **37**, 818–824 (1999).

[9]Y. Aurégan, M. Leroux, and V. Pagneux, "Measurement of liner impedance with flow by an inverse method," AIAA Paper No. 2004-2838 (2004).

[10]T. Elnady and H. Bodén, "An inverse analytical method for extracting liner impedance from pressure measurements," AIAA Paper No. 2004-2836 (2004).

[11]M. Taktak, J.-M. Ville, M. Haddar, G. Gabard, and F. Foucart, "A 3D multiport scattering matrix based-method for educing wall impedance of cylindrical lined duct section: Simulation and error evaluation," Adv. Acoust. Vib. **2009**, 928367 (2009).

[12]W. Eversman and J. Gallman, "Impedance eduction with an extended search Procedure," AIAA Paper No. 2009-3235 (2009).

[13]Y. Aurégan, R. Starobinski, and V. Pagneux, "Influence of grazing flow and dissipation effects on the acoustic boundary conditions at a lined wall," J. Acoust. Soc. Am. **109**, 59–64 (2001).

[14]E. J. Brambley, "Viscous boundary layer effects on the Myers impedance boundary condition," AIAA Paper No. 2009-3241 (2009).

[15]H. Schlichting, *Boundary Layer Theory* (McGraw-Hill, New York, 1979), pp. 603–608.

[16]R. Kumaresan and D. Tufts, "Estimating the parameters of exponentially damped sinusoids and pole-zero modeling in noise," IEEE Trans. Acoust., Speech, Signal Process. **30**, 833–840 (1982).

[17]X. Jing, S. Peng, and X. Sun, "A straightforward method for wall impedance eduction in a flow duct," J. Acoust. Soc. Am. **124**, 227–234 (2008).

[18]Y. Li, K. Liu, and J. Razavilar, "A parameter estimation scheme for damped sinusoidal signals based on low-rank hankel approximation," IEEE Trans. Signal Process. **45**, 481–486 (1997).